Materials Today Advances 4 (2019) 100028

Contents lists available at ScienceDirect

Materials Today Advances

journal homepage: www.journals.elsevier.com/materials-today-advances/

# New network architectures with tunable mechanical properties inspired by origami

N. Yang [a, *], Y. Deng [a], Z.F. Mao [a], Y.T. Chen [a], N. Wu [b], X.D. Niu [a]

[a] Intelligent Manufacturing Key Laboratory of Ministry of Education, Shantou University, Shantou 515063, China
[b] Department of Mechanical Engineering, University of Manitoba, Winnipeg, Manitoba, Canada R3T 5V6

ARTICLE INFO

*Article history:*
Received 9 August 2019
Received in revised form
15 October 2019
Accepted 21 October 2019
Available online xxx

*Keywords:*
Porous structures
Lattice structures
Folding mechanism
Force responses
Additive manufacturing

ABSTRACT

From chemistry-based methods to physics-based methods, there are many techniques to construct porous scaffolds for use in tissue engineering. Among them, computer-aided design (CAD) methods combined with additive manufacturing techniques are promising because they allow accurate control of complex scaffold morphology. Inspired by an ancient art, origami, we propose a novel CAD solution for building porous scaffolds with adjustable overall topologies and mechanical properties tuned by the origami-based parameters. Here, we mainly focus on (1) how to obtain a network from an origami structure and how to fabricate it, (2) how to change the network's topology and mechanical properties by tuning the folding angles and plane angles. With the same porosity, it has been demonstrated that the origami-inspired network's stiffness, yield strength, and ultimate compressive strength are much higher than those of other reported networks, which results from the architecture designed by the origami-inspired design concept. This interesting concept can bridge the gap between origami-based networks and load-bearing orthopedic applications with mechanical biomimetic design, but it is not limited to medical applications.



## 1. Introduction

An ideal combination of stiffness and porosity is critical for supporting tissues and culturing cells. With sufficient force support, an appropriate environment is expected to be created for contacts between cells and interactions between the extracellular matrix and cells, which is in favor of cell survival, proliferation, and differentiation [1–7]. There are many methods for generating porous media, including traditional chemistry-based methods, such as phase separation [1] and salt leaching [2], and promising physics-based methods, such as CAD-AM strategies [3]. Likewise, there are many different CAD methods for construction of porous architectures, such as direct lattice construction [4,5], the triply periodic minimal surfaces method [6], and the implicit-surface–based method [7]. However, the current pore-making methods slightly change the structure's overall topology. For example, one common method of increasing the stiffness is to decrease the porosity by increasing the strut radius in a network [4–7]. Fortunately, current origami/kirigami-based design method [8] and hierarchical lattice construction technique [9] show that flexible mechanical properties and functionalities can be achieved by using mechanism-based and topological materials [10].

Here inspired by the ancient East Asian art of origami [8,11,12], we propose an interesting construction concept for designing porous scaffolds with tunable mechanical responses. Here, both the topologies and mechanical behaviors can be effectively controlled by unique origami-based parameters, such as plane angles and folding angles instead of only porosity. Thus, it may open new avenues for expanding the range of mechanical properties of implants to be chosen for load-bearing orthopedic applications. More than that, the strong yet light property of the origami-inspired network structure is highly desirable in aerospace and automotive industry.

In the following, this research will mainly focus on (1) how to obtain a network from an origami structure and how to fabricate it, (2) how to change the network's topology referencing the deformation of its origami counterpart, (3) how to change its mechanical properties with the origami-based parameters. Finally, our origami-based networks are compared with the networks proposed in Ref. [13], and their mechanical behaviors are interpreted using finite element analysis.

* Corresponding author.
*E-mail address:* nyang@stu.edu.cn (N. Yang).

https://doi.org/10.1016/j.mtadv.2019.100028

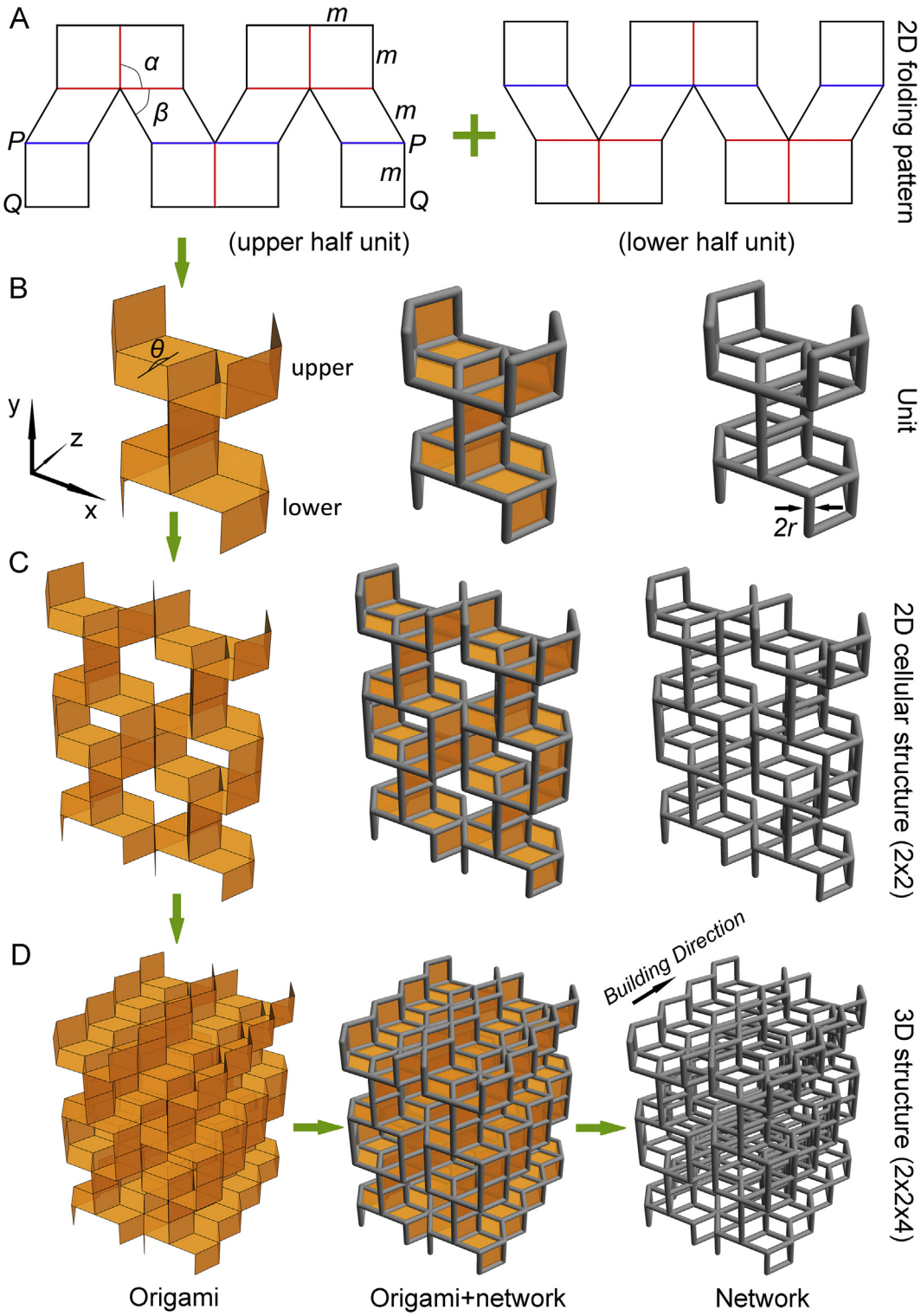


**Fig. 1.** Design process of the origami-inspired porous architecture. A: 2D folding pattern of a half unit. B: One unit is symmetrically assembled by two half units. C: 2D cellular architecture with $2 \times 2$ units. D: 3D cellular architecture with $2 \times 2 \times 4$ units created by stacking 2D cellular architectures along Z direction (also the building direction in selective laser melting). The green arrows show the overall design flow.

## 2. Materials and methods

### 2.1. Scaffold design flow

Design process of the origami-inspired porous architecture is shown in Fig. 1. First, we make a 3D foldable structure from a 2D sheet. Fig. 1A shows the 2D folding pattern on a plane, where the black lines need to be cut, and the red lines are mountain creases and the blue lines are valley creases, and the two edges marked as "PQ" need to be connected. After assembling the upper and lower half unit, a 3D unit is formed as shown in Fig. 1B (see the left structure). By replicating units in the x-y plane, a 2D cellular

**Table 1**
Measured sizes of samples in x, y, z direction.

| Sample ($\theta^{\circ}$,$\beta^{\circ}$,porosity) | x (mm) | y(mm) | z(mm) | Strut diameter(mm) |
|---|---|---|---|---|
| #1(180,45,92%) | 21.28±0.02 | 18.2±0.04 | 15.03±0.03 | |
| #2(180,60,92%) | 21.26±0.01 | 16.04±0.01 | 18.24±0.01 | |
| #3(180,75,92%) | 21.21±0.03 | 13.57±0.05 | 20.25±0.01 | |
| #4(90,60, 92%) | 29.29±0.01 | 15.36±0.01 | 12.93±0.01 | 0.58±0.02 |
| #5(240,60,85%) | 14.48±0.01 | 15.3±0.02 | 15.79±0.01 | |
| (180,60,75%) | 21.98±0.01 | 16.75±0.01 | 18.63±0.03 | 1.34±0.01 |
| (180,60,70%) | 22.12±0.02 | 16.92±0.02 | 18.78±0.02 | 1.46±0.02 |

structure can be constructed (the left structure in Fig. 1C). By then stacking such 2D structures along the Z direction, a 3D cellular architecture with facets can be created (the left structure in Fig. 1D). By replacing the creases with cylinder rods (middle structure in Fig. 1D) and removing all facets, the porous networks are finally obtained (right in Fig. 1D). The green arrows indicate the design flow.

For controlling the overall geometry of a unit, two plane angles $(\alpha, \beta)$, one folding angle $(\theta)$, length $(m)$, and the rod radius $(r)$ are defined in Fig. 1. Here, we intend to investigate the influences of only origami-based parameters ($\beta$ and $\theta$) with $\alpha = 90^{\circ}$ on the mechanical properties, thus $m$ and $r$ are kept as constants. See more details of unit cell geometry of origami structure in Appendix.

### 2.2. Scaffold fabrication

After exporting the 3D networks as STL files, the porous scaffold samples were fabricated using selective laser melting technique with medical stainless-steel powder (304 stainless-steel, particles ranged from 10 to 45 μm) with building direction as shown in Fig. 1D. A 275W laser with energy density of 104 J/mm$^3$ was applied and the laser spot diameter was 70 μm. Then, the samples were cut from the substrate using wire electrical discharge machining wire-cutting and then sand-blasted.

### 2.3. Compression testing

In the quasi-static compression testing, a 50 KN universal force-testing machine was applied, and all samples were loaded at a constant speed of 2 mm/min to failure. Three replicates of each designed scaffold were tested. The stiffness is defined by the maximum slope of the stress-strain curve in the linear elastic region according to ISO-13314 standard, and the yield strength is defined by 0.2% offset method [13].

**Table 2**
Mechanical properties of origami-based networks (Z direction) and samples in Ref. [10] (in light blue region).

| Sample ($\boldsymbol{\theta}^{\circ}$,$\boldsymbol{\beta}^{\circ}$) | Designed porosity (%) | Measured porosity (%) | Stiffness (GPa) | 0.2% offset strength (MPa) | First maximum strength (MPa) |
|---|---|---|---|---|---|
| #1(180,45) | 92 | 91.6±0.15 | 0.085±0.015 | 7.65±0.15 | 22.8±0.4 |
| #2 (180,60) | 92 | 92.3±0.17 | 0.105±0.005 | 10.01±3 | 10.3±0.7 |
| #3(180,75) | 92 | 92.4±0.04 | 1.12±0.4 | 10.48±2 | 16.5±1 |
| #4(90,60) | 92 | 91±0.015 | 0.036±0.0004 | 4.76±0.09 | 6.1±0.38 |
| #5(240,60) | 85 | 86.5±0.05 | 0.1±0.01 | 10.01±0.2 | 12.4±0.1 |
| (180,60) | 70 | 66±0.2 | 6.4±0.1 | 164.9±2.7 | 476.8±3 |
| (180,60) | 75 | 71.2±0.2 | 5.8±0.4 | 110.5±2.5 | 313.2±3 |
| Tetrahedron | 70 | - | 2.9±0.1 | 88±4 | 120±4 |
| Tetrahedron | 75 | - | 1.9±0.1 | 57±8 | 68±3 |
| Octet truss | 70 | - | 1.4±0.2 | 31±2 | 31±2 |
| Octet truss | 75 | - | 1.2±0.4 | 34±11 | 39±3 |

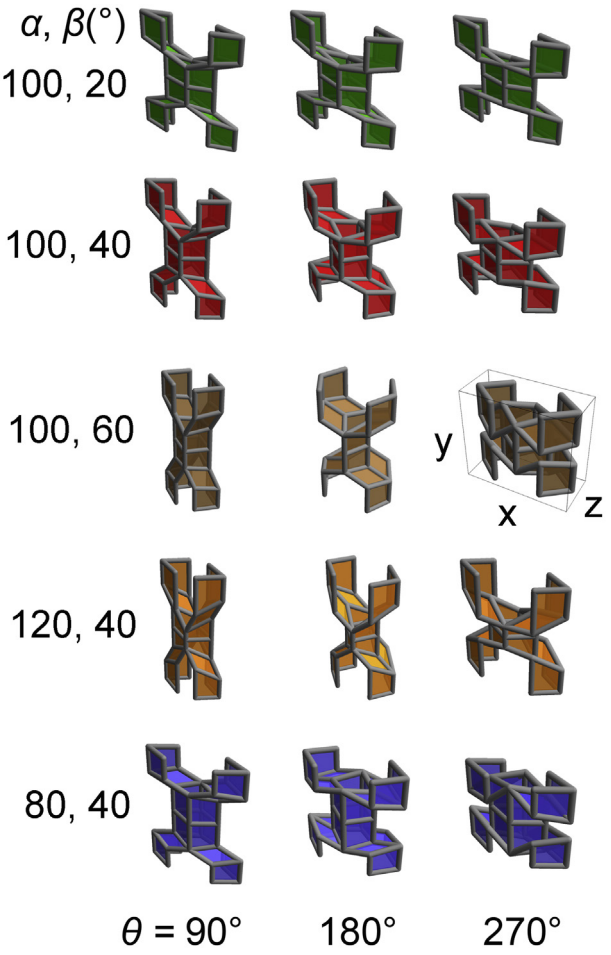


**Fig. 2.** The origami-inspired networks (made with gray struts) shown with their origami counterparts (made with facets). Structures tuned by $(\beta,\theta)$, where $\alpha = 100°$, and $\beta = 20°$ (green), 40° (red), and 60° (brown). Structures tuned by $(\alpha,\theta)$ where $\beta = 40°$, and $\alpha = 80°$ (blue), 100° (red), and 120° (orange). Folding angles are $\theta = 90°$, 180°, and 270°. The third configuration of the brown unit defines the sizes $(x, y, z)$.

### 2.4. Calculation of porosity

The volume of each designed network was directly calculated using Rhinoceros software 5.0. For the tested samples, the network volume ($V_n$) was obtained by

$V_n = M_n/\rho_n$, where $M_n$ and $\rho_n$ denote the mass of the sample and the density of the applied material ($\rho_n = 7.8 g/cm^3$), respectively.

Based on the following method, both the calculated and tested porosity were obtained.

First, the volume fraction was defined as the ratio of the network volume ($V_n$) to the corresponding total cubic solid volume ($V_{solid}$) as $Volume\ Fraction = V_{network}/V_{solid}$. Then, the porosity was obtained by subtracting volume fraction from 100% as $Porosity = 100\% - Volume\ Fraction$.

### 2.5. The measurement results and errors

In Tables 1 and 2, the result form is shown as $a \pm b$, where $a$ denotes the average value of three samples fabricated, and $b = \frac{M_{max}-M_{min}}{2}$ ($M_{max}$ and $M_{min}$ denote the maximum and minimum measurement value, respectively).

### 2.6. Finite element analysis

Finite element analysis (FEA) of the different networks is conducted in ANSYS 19 to study the unit cell deformation mechanism as well as stress–strain relationship and distribution under compression loads. For each unit cell, the 3D line structure is first modeled in Mathematica 11.2. The 3D model is then imported to ANSYS APDL as a frame, and each line of the structure is considered and modeled as a beam with the element, BEAM 189 (a 3 nodes beam element). All beams have the same circular cross-section to simulate the struts. The element size during meshing is defined as one-tenth of the size of each beam considering the calculation accuracy after convergence study.

During FEA, static structure analysis is performed considering the possible large deformation nonlinearity (nonlinearity convergence check is turned on in ANSYS). During the simulation, to match the experiment setup, all bottom notes of unit cells are fixed with zero displacement, whereas notes on the top of the structure are subjected to the same displacement along Z direction. The displacement applied to the unit cell is changed from 0 to 5% strain (elastic region). At different displacement, the stress is derived by the reaction force divided by the covering area of the unit cell on X–Y plane.

## 3. Results

### 3.1. Networks with their origami counterparts

To better exhibit the geometrical variety of the origami-inspired networks, Fig. 2 shows the relationship between the network structures and their origami counterparts with different parameter sets $(\alpha,\beta,\theta)$. The origami structures were made with facets, whereas the origami-based networks were generated by replacing the creases in the origami counterparts with struts. Simultaneously, the corresponding cubic volume of a unit with X, Y, and Z size is shown at the 3rd row and 3rd column in Fig. 2.

### 3.2. Sample fabrication

To show that this method has the capability to construct porous scaffolds of high porosity, we designed and fabricated origami-based networks with porosity of 85% and 92%. Moreover, samples with 70% and 75% porosity were made to compare their mechanical properties with the networks in Ref. [13] with the same porosity. The sizes of fabricated samples are shown in Table 1 with acceptable errors. Table 2 shows that the measured porosity basically agrees with the designed porosity, and the differences between them attribute to the forming angles of struts with respect to the building plane in 3D printing [13], the effects of internal porosity [14], sandblasting, and adhesive powders. The sandblasting process slightly increases the porosity of a sample, but it can enhance the surface roughness that is good for cell adhesion.

### 3.3. Tunable mechanical properties

In a logical manner, five kinds of samples with $\alpha = 90°$, $r = 0.27mm$, and $m = 2.5mm$ as constants and $(\theta,\beta)$ as variables were fabricated. As shown in Fig. 3A, grids 1, 2, and 3 contain samples with $\theta = 180°$ and different $\beta = 45°$, 60°, and 75°, respectively; grids 4, 2, and 5 contain samples with $\beta = 60°$ and different $\theta = 90°$, 180°, and 240°, respectively. The stress–strain curves of samples #1~#5 are shown in Fig. 3B and C when compressing the samples along the Z-axis as shown in the inserts (see also Fig. 1B for Z direction). Interestingly, the stress–strain curves begin with a linear region, and then followed by stress oscillations

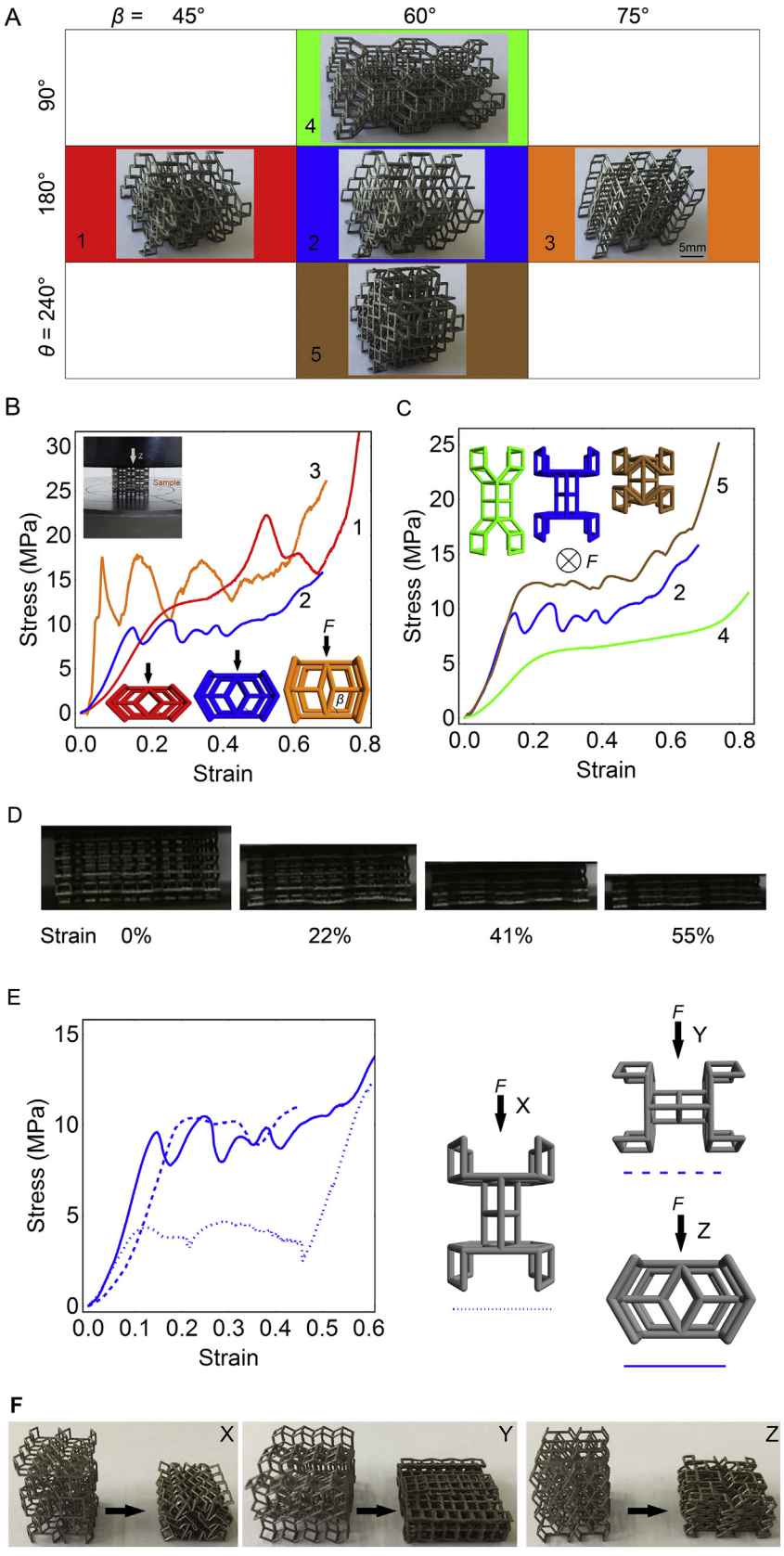


**Fig. 3.** Tunable mechanical properties of the origami-inspired networks. A: Five fabricated porous scaffolds with their geometrical parameters $(\beta, \theta)$ with $\alpha = 90°$, $m = 2.5$mm, and $r = 0.27$mm. B: Stress–strain curves with $\beta = 45°$ (red), 60° (blue), and 75° (orange) with $\theta = 180°$. C: Stress-strain curves with $\theta = 90°$ (green), 180° (blue), and 240° (brown) with $\beta = 60°$. Inset: the configuration of each sample when compressed. D: The photographs of a compressed sample with different strains. E: The anisotropic stress–strain curves of the sample with $\theta = 180°$ and $\beta = 60°$. The right part: compression of a unit along each direction (X: dotted curve, Y: dashed curve, and Z: solid curve). F: Three failure forms of a sample compressed along X, Y, and Z direction.

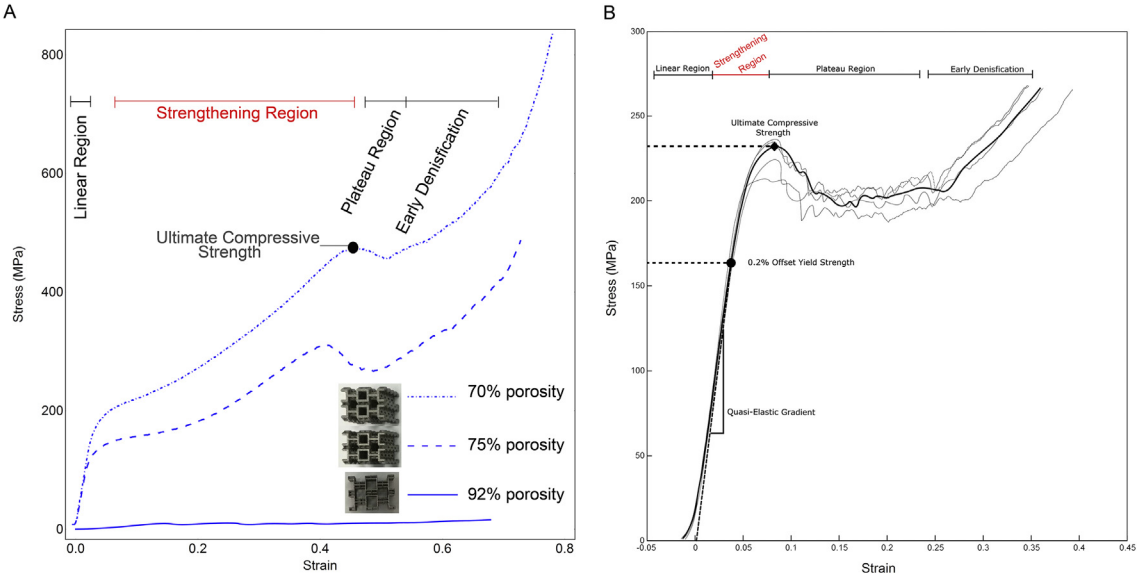


**Fig. 4.** Comparison of mechanical properties between our networks and samples in Ref. [10]. A: Our origami-inspired networks (solid curve: 92% porosity, dashed curve: 75% porosity, dot-dashed curve: 70% porosity). B: Octet truss of 50% porosity (Fig. 7 in Ref. [10]).

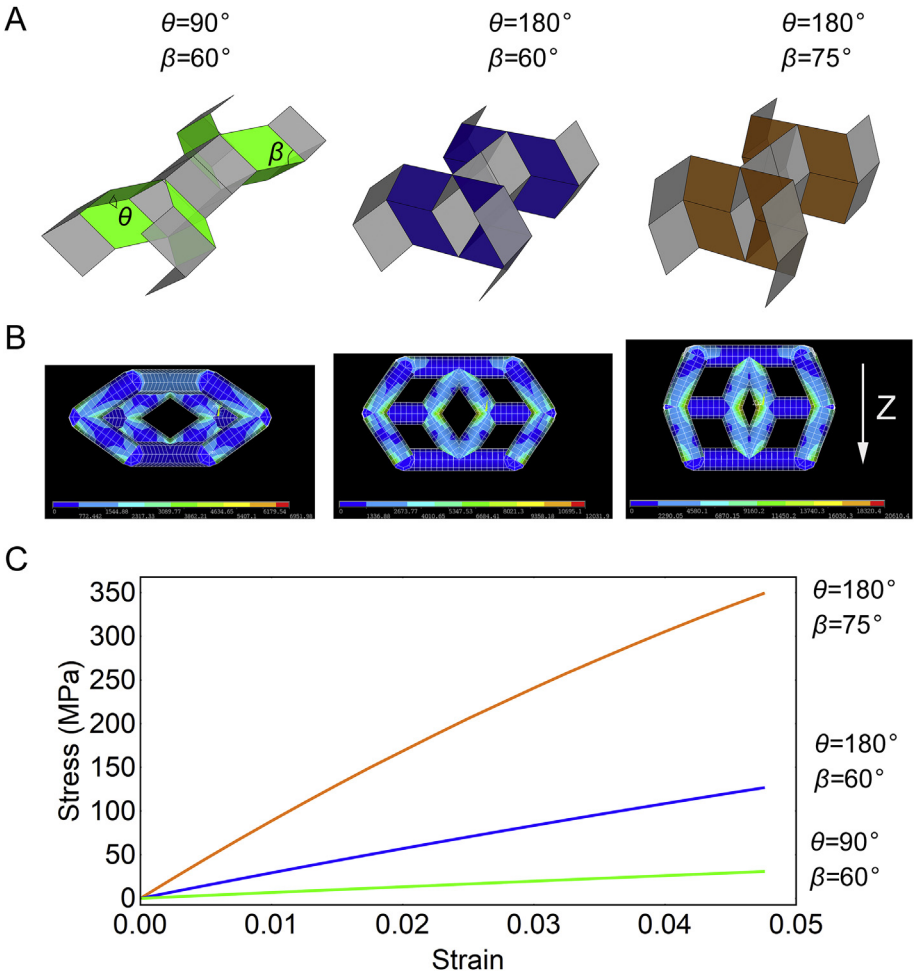


**Fig. 5.** Finite element analysis results. A: Three original origami units. B: Stress distributions in the three network units at 5% strain. C: Stress–strain curves of the three network units.

(orange and blue curve in Fig. 3B, brown curve in Fig. 3C), which shows a layer-by-layer collapse similar to the multistability effect of their origami counterparts [11,12]. Meanwhile, the sample with a small value of $\beta$ (red curve in Fig. 3B) or $\theta$ (green curve in Fig. 3C) presents less stress oscillations (like that of full-dense materials), smaller stiffness and yield strength (see Table 2). In addition, all samples are densified with monotonically increasing of stress. The order of stiffness is sample #4 ($\theta = 90°$, $\beta = 60°$, green) < sample #1 ($\theta = 180°$, $\beta = 45°$, red) < sample #5 ($\theta = 240°$, $\beta = 60°$, brown) < sample #2 ($\theta = 180°$, $\beta = 60°$, blue) < sample #3 ($\theta = 180°$ $\beta = 75°$, orange). For the five kinds of samples, we can see five fundamentally different stress–strain responses, which indicate that the mechanical properties can be tuned by the origami-based parameters.

To our surprise, among all samples from #1 to #5, sample #5 has the lowest porosity but lower stiffness than #2 and #3. This is because that, samples #2 and #3 with $\theta = 180°$ have many facets paralleling to the loading direction and directly resisting the compression. Thus, the stiffness of a network is related not only to porosity but also to the specific structural pattern.

Also, the anisotropic mechanical properties of the origami-based networks were studied in this research. The samples with $\theta = 180°$ and $\beta = 60°$ were compressed in X, Y, and Z direction and presented three different stress–strain responses. Fig. 3E shows that for stiffness, Z direction (0.105±0.005 GPa) > Y direction (0.074±0.006 GPa) > X direction (0.047±0.005 GPa), and for ultimate compressive strength (defined as the first peak of the stress-strain curve), Y direction (10.6±0.5 MPa) > Z direction (10.3± 0.7 MPa) >X direction (4.4±0.9 MPa). Similar to the mechanical properties of the origami counterparts [11,12], that of origami-based networks are anisotropic. The failure forms along the three directions are shown in Fig. 3F.

The samples with 70% and 75% porosity (with $(\beta, \theta) = (60°, 180°)$) were compressed. We find that with the same porosity, our network's stiffness, yield strength, and ultimate compressive strength are around 3, 2, and 5 times higher than those of tetrahedron, which is the stiffest structure in Ref. [11]. For example, with 75% porosity, the average values of stiffness, yield strength, and ultimate compressive strength of origami-based networks are 5.8 GPa, 110.5 MPa, and 313.2 MPa, respectively (see Table 2), whereas those of tetrahedron are 1.9 GPa, 57 MPa, and 68 MPa [11]. The origami-based structure with 75% porosity (5.8 GPa stiffness, Table 2) is even stiffer than tetrahedron with 50% porosity (4.3 GPa stiffness) [11]. In addition, our networks have relatively higher ultimate compressive strength (476.8 MPa with 70% porosity, Table 2) comparing with tetrahedron (219 MPa with 50% porosity) and octet truss (228 MPa with 50% porosity) [11], as they experience a very long strengthening region during compression, which can be seen in Fig. 4 A and B (the red region). This also implies that the origami-based networks have stronger ability of energetic absorption, which can be used as implants in the great-impact region in the body.

### 3.4. Finite element analysis

To straightforward understand the tunable mechanical properties with geometrical parameters, three origami units are show in Fig. 5A. We can see that angle $\theta \neq 180°$ makes the green facets easy to fold with a low stiffness, whereas $\theta = 180°$ makes the whole structure stiff (see the blue and orange facets). A large value of angle $\beta$ can build nearly vertical struts with a high stiffness (e.g., $\beta = 75°$). This analysis agrees with the finite element simulation results of compressions of the corresponding networks. Fig. 5B shows the Von-misses stress distributions of the three corresponding network units under 5% strain along Z direction with $r/m = 1/5$. It can be seen that in all three units, the maximum stress occurs at the inner joints of the network structures, whereas the stress are continuum at all beam connections (the beams are physically connected, they just looks separated due to the plot of the beam elements). For the units $(\beta, \theta) = (60°, 180°)$ and $(\beta, \theta) = (75°, 180°)$, the stress concentration at the top and bottom inner joints are not that obvious as the ones occur at the left and right inner joints, and the oblique (nonhorizontal) struts bear more stresses. But for the unit $(\beta, \theta) = (60°, 90°)$, stress concentrations at all inter joints are close to each other showing a relatively more uniform stress distribution at structure joints for the current strain level studied. Fig. 5C shows the stress–strain curves of the three network units. We can see that the unit with $\theta = 180°$ and $\beta = 75°$ (orange line) possesses the highest stiffness, whereas the one with $\theta = 90°$ and $\beta = 60°$ (green line) is the softest. This implies that large values of $\theta$ and $\beta$ can improve the origami-inspired network's mechanical properties (such as stiffness and strength).

## 4. Discussion

Although origami-inspired scaffolds have been demonstrated to be stiffer than other structures, high stiffness sometimes is not a merit for implants because of the stress-shielding phenomenon. To mechanically mimic native tissues, both geometric elements and fabrication parameters (such as laser power, scan speed and forming direction) [13–15] can be tuned. Meanwhile, transferring cell metabolites and delivering drugs or growth factors to cells are equally important. Therefore, the biocompatibility of the origami-inspired networks and the cell-drug-scaffold interaction need to be further investigated. Besides serving as medical implants, the origami-based networks can potentially make lightweight structures with robust mechanical properties for use in other industries, such as aerospace and automotive.

Here, we focus on experiment/analysis to initially understand the mechanical behaviors of the origami-inspired networks. In the future, we need to optimize the mechanical properties by applying numerical methods (e.g., Gibson–Ashby model and the finite element analysis method [16]) to adjust the designed scaffolds to the desired properties of a specific tissue.

## 5. Conclusion

A novel design method of porous scaffolds inspired by origami has been proposed and can be summarized thusly: origami structures are first folded/constructed from a thin sheet, and then the “creases” are replaced with struts and all facets are removed to form network architectures for further 3D printing. Moreover, the origami-based networks have been successfully fabricated using selective laser melting technique. It is found that the origami-inspired structures characterize anisotropic mechanical properties in three directions, and they can be largely tuned by the origami-based parameters (folding angles and plane angles). With the same porosity, the origami-based networks can be stiffer than other kinds of networks. This new design conception, tuning mechanical properties by geometrical elements, may offer more success than conventional methods for porous bone implant materials.

## Data availability

The experimental results are available on request.

## Declaration of competing interest

The authors declare that they have no known competing financial interests or personal relationships that could have appeared to influence the work reported in this paper.

## Acknowledgments

The authors acknowledge the National Natural Science Foundation of China (Nos. 11872046, 11772197), Tianjin Science Key Funding (14JCZDJC39500, 18JCZDJC10030), and the Scientific Research Funding of Shantou University (NTF19012). N. Yang acknowledges the support from the Young and Middle-aged Teacher Culture Program of Tianjin.

## Appendix A. Supplementary data

Supplementary data to this article can be found online at https://doi.org/10.1016/j.mtadv.2019.100028.

## References

[1] P. Fabbri, V. Cannillo, A. Sola, A. Dorigato, F. Chiellini, Highly porous polycaprolactone-45S5 Bioglass® scaffolds for bone tissue engineering, Compos. Sci. Technol. 70 (2010) 1869–1878.
[2] V. Cannillo, F. Chiellini, P. Fabbri, A. Sola, Production of Bioglass® 45S5 – polycaprolactone composite scaffolds via salt-leaching, Compos. Struct. 92 (2010) 1823–1832.
[3] L. Elomaa, S. Teixeira, R. Hakala, H. Korhonen, D.W. Grijpma, J.V. Seppälä, Preparation of poly(e-caprolactone)-based tissue engineering scaffolds by stereolithography, Acta Biomater. 7 (2011) 3850–3856.
[4] A. Pasko, O. Fryazinov, T. Vilbrandt, P.A. Fayolle, V. Adzhiev, Procedural function-based modeling of volumetric microstructures, Graph. Model. 73 (2011) 165–181.
[5] L. Wu, J. Virdee, E. Maughan, A. Darbyshire, G. Jell, M. Loizidou, M. Emberton, P. Butler, A. Howkins, A. Reynolds, I.W. Boyd, M. Birchall, W. Song, Stiffness memory nanohybrid scaffolds generated by indirect 3D printing for biologically responsive soft implants, Acta Biomater. 80 (2018) 188–202.
[6] D.J. Yoo, Porous scaffold design using the distance field and triply periodic minimal surface models, Biomaterials 32 (2011) 7741–7754.
[7] N. Yang, S. Wang, L. Gao, Y. Men, C. Zhang, Building implicit-surface-based composite porous architectures, Compos. Struct. 173 (2017) 35–43.
[8] J.T.B. Overvelde, T.A. de Jong, Y. Shevchenko, S.A. Becerra, G.M. Whitesides, J.C. Weaver, C. Hoberman, K. Bertoldi, A three-dimensional actuated origami-inspired transformable metamaterial with multiple degrees of freedom, Nat. Commun. 7 (2016) 10929.
[9] Q. Ma, H. Cheng, K. Jang, H. Luan, K.C. Hwang, J.A. Rogers, Y. Huang, Y. Zhanga, A nonlinear mechanics model of bio-inspired hierarchical lattice materials consisting of horseshoe microstructures, J. Mech. Phys. Solids 90 (2016) 179–202.
[10] K. Bertoldi, V. Vitelli, J. Christensen, M.V. Hecke, Flexible mechanical metamaterials, Nature Reviews Materials 2 (2017) 17066.
[11] H. Yasuda, J. Yang, Reentrant origami-based metamaterials with negative Poisson's ratio and bistability, Phys. Rev. Lett. 114 (2015) 185502–185505.
[12] M. Schenk, S. Guest, Geometry of miura-folded metamaterials, Proc. Natl. Acad. Sci. U.S.A. 110 (2013) 3276–3281.
[13] S. Arabnejad, R.B. Johnston, J.A. Pura, B. Singh, M. Tanzer, D. Pasini, High-strength porous biomaterials for bone replacement: a strategy to assess the interplay between cell morphology, mechanical properties, bone ingrowth and manufacturing constraints, Acta Biomater. 30 (2016) 345–356.
[14] C. Bonatti, D. Mohr, Smooth-shell metamaterials of cubic symmetry: anisotropic elasticity, yield strength and specific energy absorption, Acta Mater. 164 (2019) 301–321.
[15] S. Van Bael, G. Kerckhofs, M. Moesen, G. Pyka, J. Schrooten, J.P. Kruth, Micro-CT-based improvement of geometrical and mechanical controllability of selective laser melted Ti6Al4V porous structures, Mater. Sci. Eng. A 528 (2011) 7423–7431.
[16] D.W. Abueidda, M. Elhebeary, C.S. Shiang, S. Pang, R.K.A. Al-Rub, I.M. Jasiuk, Mechanical properties of 3D printed polymeric Gyroid cellular structures: experimental and finite element study, Mater. Des. 165 (2019) 107597.